2021 SCEC progress report for Shaw

"Developing earthquake simulators for use in seismic hazard estimates: Buried ruptures and implications for source and ground motions"

Bruce E. Shaw ,

Lamont Doherty Earth Observatory, Columbia University

We report here on progress made in the last year. One paper was published, and one paper was submitted. The first one, (*Milner, Shaw, et al., 2021*) was published in the Bulletin of the Seismological Society of America. The second one, (*Shaw, et al., 2020*) was submitted for publication. A third paper related to scaling relations is in preparation; some results from that are also discussed.

Published paper on non-ergodic hazard from fully deterministic physical models

"Toward Physics-Based Nonergodic PSHA: A Prototype Fully Deterministic Seismic Hazard Model for Southern California" (*Milner, Shaw, et al., 2020*)

We present a nonergodic framework for Probabilistic Seismic Hazard Analysis (PSHA) that is constructed entirely of deterministic, physical models. The use of deterministic ground motion simulations in PSHA calculations is not new (e.g., CyberShake), but prior studies relied on kinematic rupture generators to extend empirical earthquake rupture forecasts. Fully-dynamic models, which simulate rupture nucleation and propagation of static and dynamic stresses, are still computationally intractable for the large simulation domains and many seismic cycles required to perform PSHA. Instead, we employ the Rate-State Earthquake Simulator (RSQSim) to efficiently simulate hundreds of thousands of years of $M > 6.5$ earthquake sequences on the California fault system. RSQSim produces full slip-time histories for each rupture, which, unlike kinematic models, emerge from frictional properties, fault geometry, and stress transfer; all intrinsic variability is deterministic. We use these slip-time histories directly as input to a three-dimensional wave propagation code within the CyberShake platforms to obtain simulated 0.5 Hz ground motions. The resulting 3 s spectral acceleration ground motions closely match empirical ground motion model (GMM) estimates of median and variability of shaking well. When computed over a range of sources and sites, the variability is similar to that of ergodic GMMs. Variability is reduced for individual pairs of sources and sites, which repeatedly sample a single path, which is expected for a nonergodic model. This results in increased exceedance probabilities for certain characteristic ground motions for a source-site pair, while decreasing probabilities at the extreme tails of the ergodic GMM predictions. We present these comparisons and preliminary fully deterministic physics-based RSQSim-CyberShake hazard curves, as well as a new technique for estimating within- and between-event variability through simulation.

RSQSim produces full slip-time histories for each rupture, which, unlike kinematic models, emerge from frictional properties, fault geometry, and stress transfer; all intrinsic variability is deterministic. We use these slip-time histories directly as input to wave propagation codes with the Southern California Earthquake Center (SCEC) BroadBand Platform for one-dimensional models of the Earth and SCEC CyberShake for three-dimensional models to obtain simulated deterministic ground motions. Some figures illustrating some of the results are included below. Figure 1 illustrates a series of improvements made in the

source physics of the simulator to improve the propagation velocity to obtain more realistic directivity effects. These improvements, include: (1) Improving the accuracy of the stiffness matrix by considering not just the finite area of the source patch, but the finite area of the receiver patch as well. (2) Eliminating fixed sliding speed approximation during fast earthquake slip, and replacing it with slip velocity which is determined by the shear impedance relationship. (3) Rather than instantaneous stressing rate updating, introducing a time delay to stress rate updating on other elements which is motivated by a retarded green's function effect from finite wave speeds. An approximation of this effect uses a fixed delay for all elements related to the source patch dimension, to maintain a minimum of updating steps and preserve the fast algorithm. Together these source physics improvements lead to improved propagation velocity.

Figure 2 shows spectra plots of an individual event, and an ensemble of events, compared with empirical Ground Motion Models (GMMs). This gives an example of how the model ground motions are calibrated and validated against empirical observations.

Figure 3 shows an example of a full hazard curve calculated at a single site from the full simulator catalog using a full 3D velocity model in Cybershake. This illustrates a fully deterministic calculation of PSHA using the deterministic sequence of events and source motions from the siumlator, with no stochastic aspects.

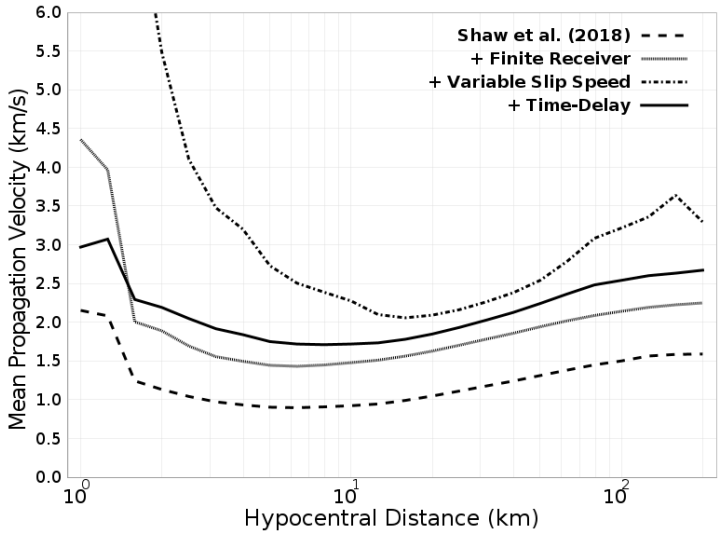

Figure 1: Propagation velocity as a function of patch hypocentral distance for four different RSQSim parameterizations, each of which incorporates a new feature over the previous model. The base model is the catalog used in *Shaw et al.* (2018), plotted with a dashed line. The first modification, plotted with a dotted line, adds a new finite receiver patch capability to the stiffness matrix calculations. The second modification, plotted with a dotted and dashed line, adds variable slip speed capabilities to RSQSim with stepwise updating of sliding velocity on a patch during earthquake slip. The final model, plotted with a solid line and used for PSHA calculations in this study, also includes a time-delay to the static-elastic interaction. From [Milner, Shaw, et al., 2020].

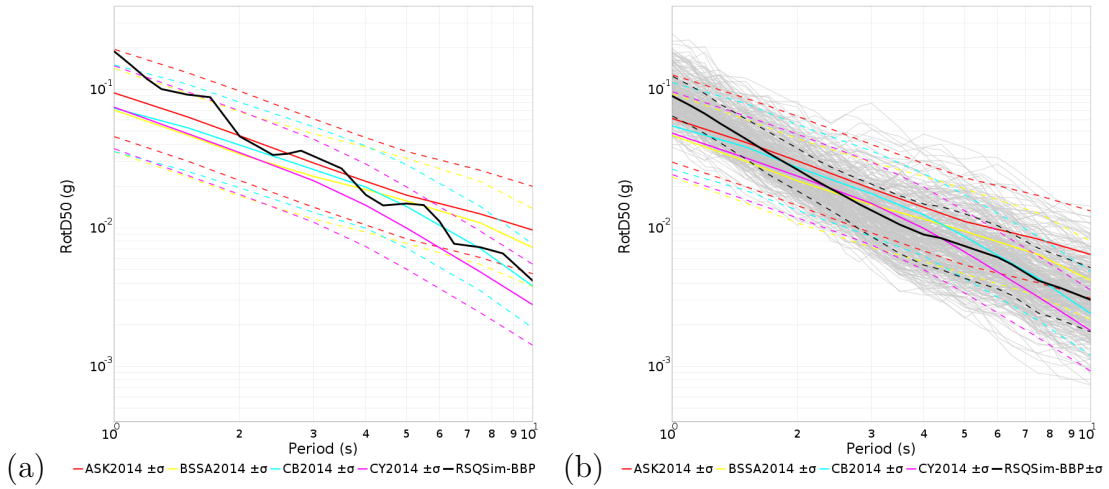

Figure 2: Example ground motions from simulator events compared with Ground Motion Models (GMM). RotD50 spectra for site USC from ruptures on the Mojave section of the San Andreas Fault, computed with a one-dimensional (1D) velocity structure with VS30=500 m/s in the Southern California Earthquake Center (SCEC) BroadBand Platform (BBP). (a) Spectrum for a M 7.48 rupture on the Mojave section of the San Andreas Fault plotted as a thick black line. (b) Spectra for 185 different $7.0 \leq M \leq 7.5$ RSQSim ruptures on the Mojave section of the San Andreas Fault simulated at USC plotted with thin gray lines, the mean of all 185 ruptures as a thick black line, and the mean plus and minus one standard deviation with dashed black lines. GMM comparisons (with plus and minus one standard deviation bounds marked with dashed lines) are plotted with colored lines. GMM predictions are slightly different for (b) because distributions are averaged across those predicted for each of the 185 RSQSim ruptures (rather than for a single M 7.48 rupture in (a)). From [Milner, Shaw, et al., 2020].

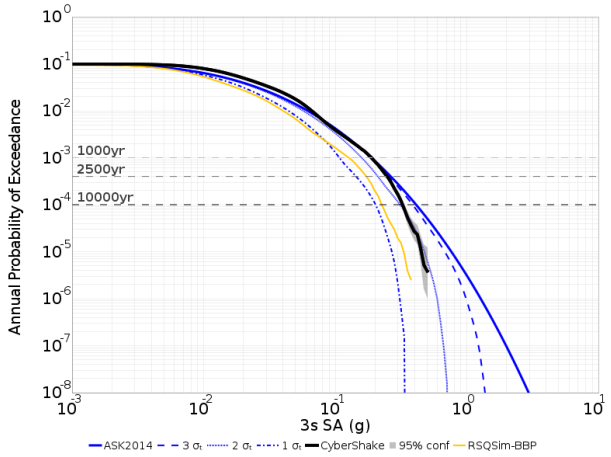

Figure 3: Example of full deterministic PSHA calculation using 3D cybershake and simulator ruptures, done at a single site. RSQSim simulation hazard curves at USC. CyberShake (3D) is plotted with thick, black lines. (a) ASK2014 GMM comparisons curves in blue, with the complete hazard curve plotted as a thick solid line. GMM curves computed from truncated log-normal distributions at three-, two-, and one-sigma are plotted with dashed, dotted, and dotted and dashed lines respectively. The 1D BBP hazard curve is included in yellow, and 95% confidence bounds assuming a binomial distribution (representing sampling uncertainty from a finite catalog duration) on the 3D simulated curve as a gray shaded region. From [Milner, Shaw, et al., 2020].

New Zealand simulator

"An Earthquake Simulator for New Zealand" (*Shaw, et al., 2021*)

We present an earthquake simulator for New Zealand. It uses the RSQSim simulator engine based on approximations of the rate-and-state friction equations. The full set of faults considered in the most recent NZ national seismic hazard map are included in the simulator. New simulator methods are introduced that allow for the inclusion and interaction between upper plate faults and a subduction interface fault below them. The simulator generates sequences of complex slip events and a catalog of finite ruptures hundreds of thousands of years in length. Results from the simulator are evaluated through statistical testing and comparison with geological and geophysical observations. These evaluations include a spatial comparison against historical earthquakes, a comparison against rates of events in the instrumental catalog, and a comparison against scaling relations. Significant aspects of the resulting synthetic catalogue are discussed. These include substantial variability over instrumental catalog timescales, and spontaneous ruptures which break both the upper crustal faults and subduction interface co-seismically. A variety of potential uses of the model are noted.

Some figures illustrating the results are included below. Figure 4 shows epicenters in the model compared with historical and instrumental catalogs. Figure 5 shows distributions of sizes of events in the model compared with the instrumental catalogs. Figure 6 shows an example multifault event where the subduction interface breaks and faults in the upper crustal plate break co-seismically. These events where the upper plate faults break co-seismically with the subduction interface are very common in the model.

Scaling relations

(Shaw, 2021, in preparation) Further work was done on using earthquake simulators to guide scaling relations. We have developed new magnitude-area scaling corrections valid across all mechanisms which corrects for aspect ratio and burial and surface effects. This scaling relation works well on the simulator ruptures. Figure 7 illustrates the dependence on different burial depths, showing changes in magnitude anomalies ($\mathbf{M} - \log_{10} A - C$ for magnitude $\mathbf{M}$ and area A and constant C) as a function of aspect ratio and depth of buried faults, for the case of a single fault. Figure 8 illustrates the fit of the new scaling relation for a complex fault system, here the California UCERF3 faults.

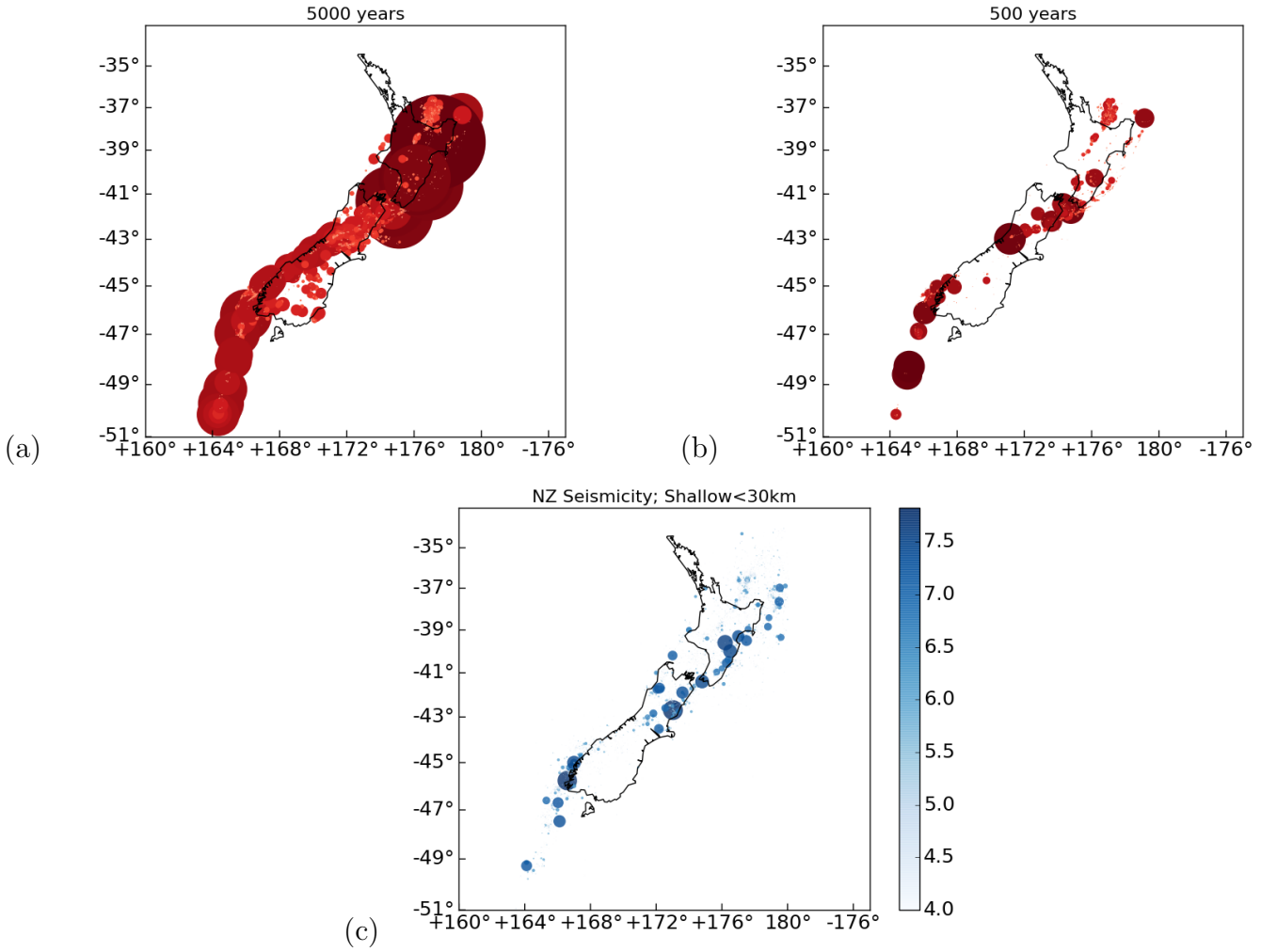

Figure 4: Epicenter map. Color and size coded by magnitude. Size scaled with area. Plotted sequentially in time, earlier smaller events may be hidden by later larger events. (a) Catalog length here is 5000 years. This is akin to long term catalog. (b) Catalog length 500 years. (c) Historical and instrumental catalog through 2020 of New Zealand earthquakes, compiled by GeoNet. Blue colormap highlights observed earthquakes. Only shallow (above 30km depth) events are plotted, since the model aims only to simulate shallow events. To first order we see spatial consistency. Some spatial differences in medium and large event productivity are seen in Central and Northern Hikurangi (in the East), with observed catalog being more productive. Also model catalog appears more productive in the Bay of Plenty (in the Northwest). From (*Shaw et al.*, 2021).

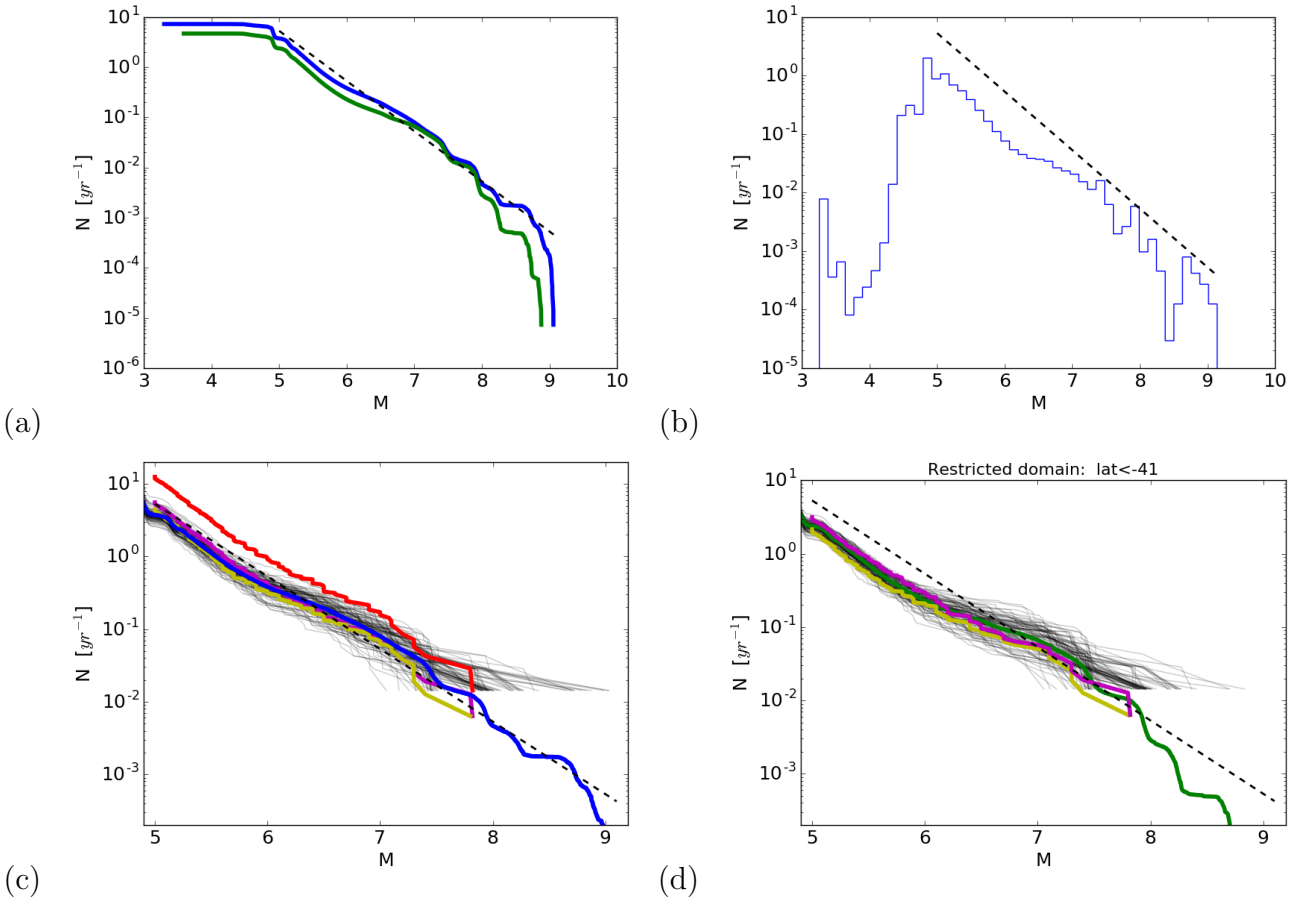

Figure 5: Distribution of sizes of events. (a) Cumulative model events. Blue line is full model; green line is latitude restricted ($< -41°$). (b) Differential model events. We see the cumulative distribution appearing fairly close to $b = 1$ here, though there are some underlying differences from that in the differential distribution. Dashed line shows $b = 1$, and has constant amplitude in all the plots to aid comparison between them. (c) Instrumental New Zealand seismicity 1940-2020. Red line is full catalog. Magenta line is reduced by a factor of 2/3 to represent anticipated on-fault rate, and an additional facotr of 2/3 for recalibration of magnitude estimates. Yellow line is restricted to exclude the last very active decade, covering the years 1940-2010. The blue line shows the mean model catalog from (a). In the background, grey lines show 100 different samples of model catalogs of 80 year lengths to show variability in productivity over the finite observational catalog timescale. The model is found to be consistent with the corrected catalog observations. (d) Test of model productivity with earthquake catalog when both are restricted to latitudes South of $-41°$, excluding subduction zone area. Magenta line shows catalog from 1940-2020. Yellow line shows catalog restricted to years 1940-2010 omitting last decade with exceptionally high activity. Model mean with green line. Grey lines show 100 different samples of model catalogs of 80 year lengths to show variability in productivity. Again consistency of model and observations is found. From (*Shaw et al.*, 2021).

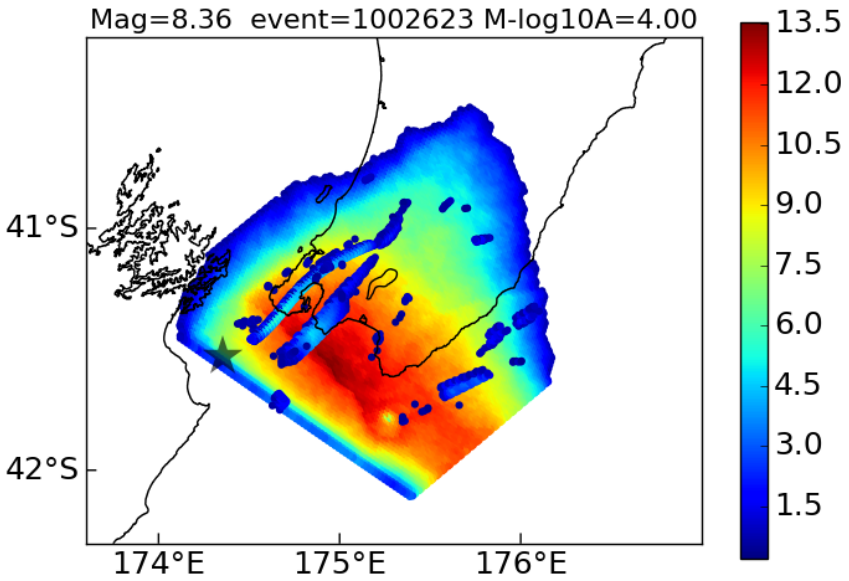

Figure 6: Map view of large **M**8.4 subduction event which also ruptures coseismically a number of upper plate faults. Main subduction fault is the Southern Hikurangi. The next largest participating faults by area are the Wellington, Wairarapa, and BooBoo faults, respectively. Color indicates slip in meters. The event initiates on the subduction interface at the epicenter indicated by the grey star. From (*Shaw et al.*, 2021).

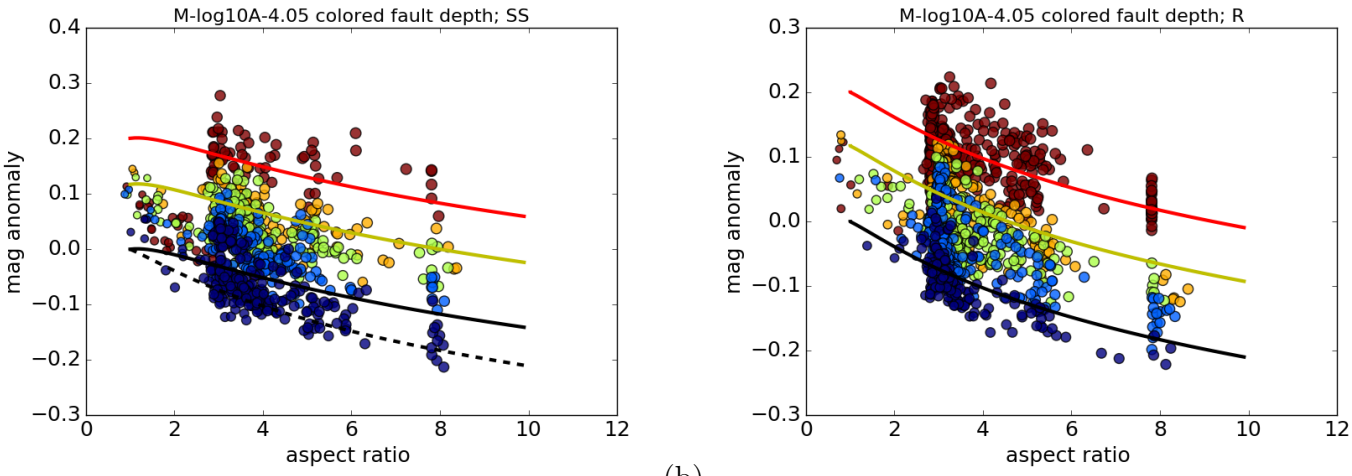

(a) (b)

Figure 7: Single dipping fault magnitude anomalies for different depth ruptures. Different colors represent different depths of burried fault. Lines show scaling relation decreased anomaly with increasing depth of ruptures. (a) Strike Slip (b) Dip Slip

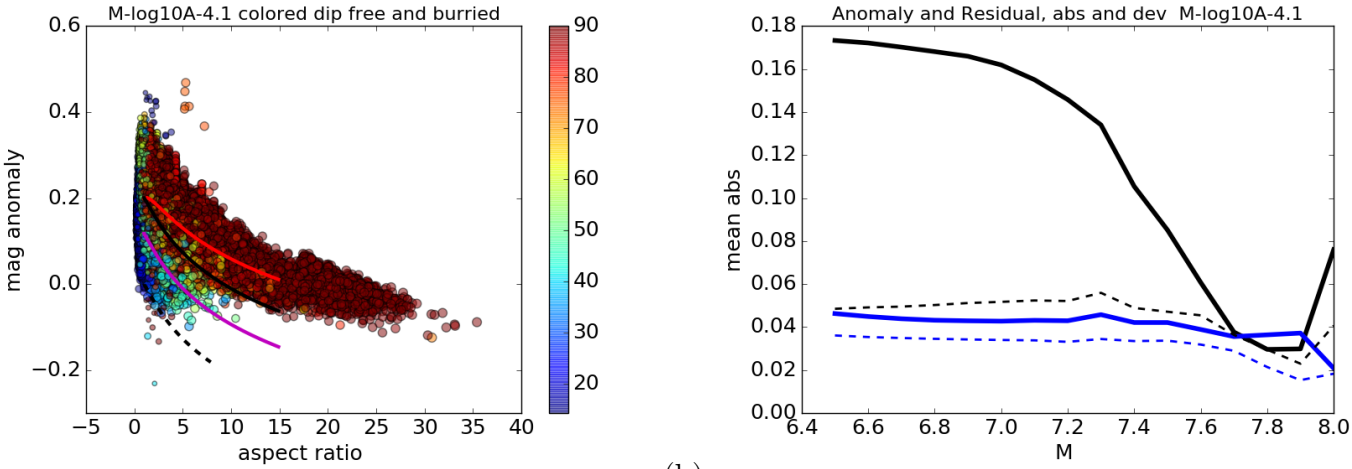

(a) (b)

Figure 8: New magnitude area scaling with corrections for aspect ratio and buried rupture effects across different mechanisms. Points are events from RSQSim simulation of UCERF3 fault system. (a) Anomaly, difference between magnitude and $\log_{10}$ area as a function of aspect ratio. Points colored by dip. (b) Average over all events of residual as a function of lower magnitude cutoff once correction is applied. once correction is applied. Solid black line is mean absolute anomaly. Solid blue line is mean absolute residual. Dashed black line is mean absolute deviation of anomaly. Dashed blue line is mean absolute deviation of residual. Note the solid blue line is close to the dashed blue line, meaning there is little bias in the remaining residual. Note also the small remaining mean absolute residual, meaning we are on average capturing most of the systematic effects with the scaling corrections being applied. From [Shaw, in preparation, 2021].

References

Milner, K. R., B. E. Shaw, C. A. Goulet, K. B. Richards-Dinger, S. Callaghan, T. H. Jordan, J. H. Dieterich, and E. H. Field, Toward Physics-Based Nonergodic PSHA: A Prototype Fully-Deterministic Seismic Hazard Model For Southern California, *Bull. Seismol. Soc. Am.*, doi:10.1785/0120200216, 2021.

Shaw, B. E., K. R. Milner, E. H. Field, K. Richards-Dinger, J. J. Gilchrist, J. H. Dieterich, and T. H. Jordan, A physics-based earthquake simulator replicates seismic hazard statistics across California, *Science Advances*, *4*, eaau0688, doi:10.1126/sciadv.aau0688, 2018.

Shaw, B. E., B. Fry, A. Nicol, and M. Gerstenberger, An earthquake simulator for New Zealand, p. preprint, 2021.